ChemComm

COMMUNICATION

View Article Online
View Journal | View Issue

Cite this: *Chem. Commun.*, 2023, **59**, 10992

Received 26th July 2023,
Accepted 7th August 2023

DOI: 10.1039/d3cc03582d

rsc.li/chemcomm

Localised polymerisation of acrylamide using single-barrel scanning electrochemical cell microscopy†

Mahir Mohammed, Bryn A. Jones, Evelina Liarou and Paul Wilson *

Single-barrel scanning electrochemical cell microscopy has been adapted for polymerisation of acrylamide in droplet cells formed at gold electrode surfaces. Localised electrochemical atom transfer radical polymerisation enables controlled synthesis and deposition of polyacrylamide or synthesis of polyacrylamide brushes from initiator-functionalised electrode surfaces.

The ability to create, control and interrogate interfaces with micro- to nanoscale resolution remains a challenge in the fields of microfabrication and nanotechnology. Top-down approaches are typically destructive and unsuitable for the patterning soft materials based on organic or biological macromolecules,[1] required for a variety of applications *e.g.* (nano)medicine,[2] (bio)electronics,[3] and cyptography.[4] Thus, the development of bottom-up, soft lithography techniques has become increasingly important. State-of-the-art techniques include micro-contact printing (μCP),[5] photolithography (PL)[6] and block copolymer self-assembly,[7] while probe-based methods such as dip-pen nanolithography (DPN),[8] polymer-pen lithography[9] offer precise control over feature resolution.

Scanning electrochemical cell microscopy (SECCM)[10] has been developed as a meniscus-based technique for high resolution synchronised electrochemical and topographical imaging enabled by integration of a probe positional feedback mechanism.[10–12] Conventional SECCM operates on dry electrode surfaces in which electrochemical cells are confined to droplets formed between an electrolyte filled dual-barrel nanopipette and the surface of interest. This configuration of SECCM has been exploited for micro- and nanoscale electrochemical patterning of surfaces.[13–16] It has also been deployed for attempted localised surface-initiated electrochemical atom transfer radical polymerisation (SI-eATRP).[17] Polymerisation of *N*-hydroxyethylacrylamide (HEAm) was realised in droplet cells formed at gold substrates modified with a self-assembled monolayer (SAM) presenting an ATRP initiator. However, using Cu^{II}/Me_6TREN at $V_{surf} < -0.5$ V (*vs.* Ag^+/AgCl) reduction of dissolved oxygen at the electrode resulted in formation of reactive oxygen species (ROS) in the droplets capable of initiating radical polymerisation which competed with the desired SI-eATRP process (Fig. 1, left). To improve control over the initiation process we have been investigating the use of less reducing Cu-complexes in laboratory-scale 'plug-and-play' simplified eATRP for translation to SECCM.[18–21]

Likewise, an operationally simplified single barrel SECCM configuration has also been developed.[11,22] Dual barrel SECCM involves application of a potential bias between quasi-reference counter electrodes (QRCEs) placed in the barrels of the probe. A voltage-wave generator (external or *via* a lock-in amplifier) is required to measure and control oscillations of the probe, sinusoidally, normal to the surface. An induced ac component

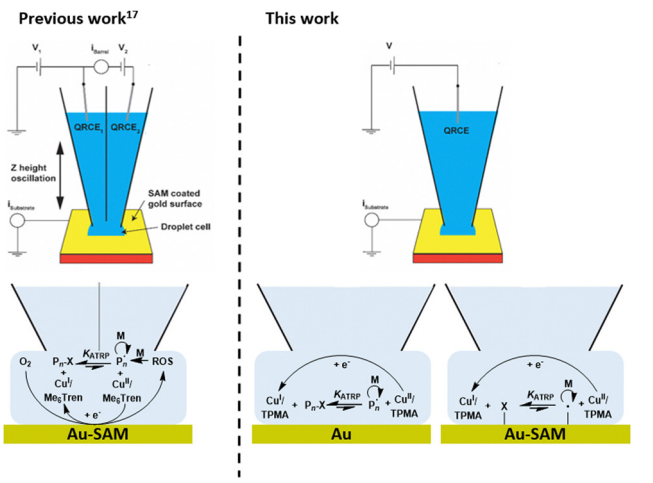

Fig. 1 Schematic showing the operationally complex dual-barrel SECCM configuration and Cu/Me_6Tren as a catalyst for localised eATRP which was found to proceed with a competing undesirable ROS-initiated mechanism (left).[17] Here we employ simplified single-barrel SECCM for the first time to control eATRP both at and from the surface of a gold electrode (right).

Department of Chemistry, University of Warwick, Coventry, CV4 7AL, UK.
E-mail: p.wilson.1@warwick.ac.uk

† Electronic supplementary information (ESI) available. See DOI: https://doi.org/10.1039/d3cc03582d

of the ionic conductance (barrel) current (i_{ac}) is then used as a feedback signal to control the distance between the end of the probe and the surface. Conversely, positional feedback in single barrel SECCM is conferred by detection to surface current (i_{surf}) only. When the nanopipette meniscus makes contact with the surface creating a two-electrode droplet electrochemical cell in which the response of i_{surf} to a reaction at a given V_{surf} can be used to monitor a reaction of interest localised to the droplet cell. This significantly simplifies the instrumentation and software required to perform experiments (*e.g.* no lock-in amplifier needed, Fig. S2, ESI†). The simplicity and ease of operation is a significant advantage in attempting microscale and nanoscale deposition,[23] and it is still possible to perform electrochemical mapping and topographical measurements.[24]

Here, we report the first use of single-barrel SECCM for eATRP of acrylamide (Am) using Cu^{II}/tris(2-pyridylmethyl)amine (Cu^{II}/TPMA), overcoming some of limitations of our previous system. At appropriate V_{surf}, eATRP enables controlled synthesis and deposition of polyacrylamide (PAm) at gold surfaces, whilst at initiator-functionalised electrode surfaces the controlled formation of PAm brushes is also possible (Fig. 1, right).

An aqueous solution of Cu^{II}/TPMA (6.9 mM) in a single barrel nanopipette (1 μm diameter) was delivered to a gold electrode surface in a 2 × 2 array (depicted in Fig. S3, ESI†). A threshold current ($i_{surf} = -1 \times 10^{-11}$ A) was set to create an electrochemical cell confined to the dimensions of the droplet formed at the electrode surface. Voltametric analysis by cyclic voltammetry (CV) revealed the onset of a reduction event at $E = -0.30$ V reaching $i_{pc} = -2.6 \times 10^{-10}$ A at $E_{pc} = -0.6$ V (Fig. S4A, ESI†). This was assigned to the reduction of Cu^{II}/TPMA to Cu^{I}/TPMA.[26,27] The absence of an oxidation peak in the anodic scan is attributed to oxidation of Cu^{I}/TPMA to Cu^{II}/TPMA by dissolved oxygen in the solution. AFM of the landing sites revealed the landing foot-print of the nanopipette but no significant feature deposition (Fig. S4B, ESI†) When acrylamide (Am) was added to the solution (10 wt%) the onset of reduction shifted to $E = -0.18$ V which is typical for aqueous solutions monomer in macroscopic CV.[25] The magnitude of the current at $E_{pc} = -0.6$ V increased to $i_{pc} = -2.6 \times 10^{-10}$ A. On one hand the increase in i_{pc} can be explained by the aqueous solution of monomer wetting the surface leading to larger droplet sizes. On the other hand, at more reducing potentials it is possible that some free radical polymerisation (FRP) of Am occurs during the CV scan which could effect the surface wettability. Indeed, AFM analysis revealed the presence of more prominent features (Fig. S4C, ESI†). Addition of 2-hydroxyethyl 2-bromoisobutyrate (HEBiB; 0.23 M) to the solution resulted in an increase in i_{pc} from -5.7×10^{-10} A to $i_{pc} = -1.4 \times 10^{-9}$ A, arising from the electrochemical reduction of Cu^{II}/TPMA to Cu^{I}/TPMA followed by fast activation of HEBiB by the *in situ* generated Cu^{I}/TPMA species.[26,27] AFM analysis revealed the formation of prominent features under these conditions (Fig. S4D, ESI†).

Voltamettric analysis (CV) performed on aqueous solutions of Am only, using KNO_3 as an electrolyte, revealed that Am was not redox active (Fig. S5, ESI†). Conversely, solutions containing Am and HEBiB in aqueous KNO_3 exhibited a reduction event at $E < -0.2$ V, which can be attributed to direct reduction of HEBiB.[28] Chronoamperometric analysis was performed on droplet cells, containing only aqueous Am and HEBiB, at gold surfaces. The potential was biased at 50 mV intervals between -0.2 V $< V_{surf} < -0.05$ V (*vs.* Ag^+/AgCl, QRCE) to generate *i vs. t* traces. Only capacitative currents were observed (Fig. S6A, ESI†). However, when Cu^{II}/TPMA was added, faradaic currents that increased with decreasing (more reducing) V_{surf} were observed, indicative of the electrochemical reduction of Cu^{II}/TPMA followed by activation of HEBiB (Fig. S6B, ESI†).

Based on the results obtained from CV and *i vs. t* measurements, reaction solutions containing [Am] : [HEBiB] : [Cu^{II}/TPMA] = [20] : [1] : [0.5] : [0.625] were prepared and loaded into single barrelled nanopipettes to be delivered to a gold electrode substrate biased to $V_{surf} = -0.15$ V. At this surface potential the time of deposition (TOD) for the proposed eATRP of PAm within the droplet cells was varied (TOD = 100–600 s). From a qualitative point of view, analysis by AFM indicated that the dimensions of the features increased with increasing TOD (Fig. 2A). After repeated experiments the average height of the features was shown to increase with increasing TOD (Fig. S7–S9, ESI†). This is indicative of well controlled eATRP of Am occurring within the droplet cells.

The applied potential was then varied with TOD fixed at 200 s. Decreasing the V_{surf} in −10 mV increments from −0.15 V

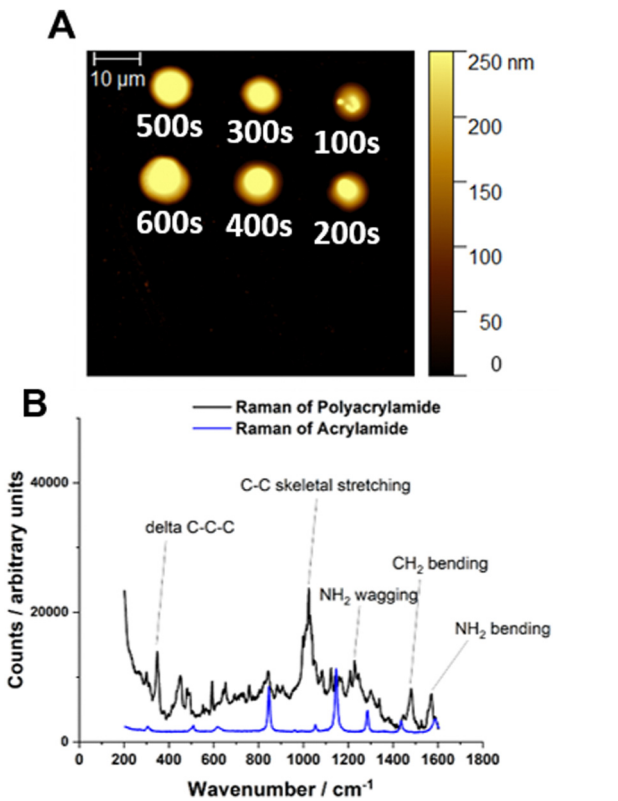

Fig. 2 For single-barrel SECCM eATRP of Am using [Am] : [HEBiB] : [Cu^{II}] : [TPMA] = [20] : [1] : [0.5] : [0.625] at room temperature; (A) AFM image of the spots deposited at $E_{app} = -0.15$ V; (B) Raman spectrum of PAm deposited during an extended TOD experiment (TOD = 1800 s; $E_{app} = -0.15$ V). Raman settings–exposure time: 600 s, laser: λ = 820 nm, power: 100%, objective: 50×, grating: 1200 l mm^{-1}, pinhole: IN.

to −0.22 V revealed little correlation between V_{surf} and the amount of PAm formed within each droplet cell (Fig. S10–S12, ESI†). We were not surprised by this result as on the laboratory scale we have shown more reducing potentials yields slower reactions, lower conversions, and poor control over the polymerisation of HEAm performed at room temperature, and lower temperatures are required to achieve electrochemical control.[21]

The amount of polymer synthesised during SECCM-based experiments limits the methods available for sample characterisation. Conventional analysis by size-exclusion chromatography (SEC) and nuclear magnetic resonance (NMR) spectroscopy is not possible. In our previous work with used X-ray photoelectron spectroscopy (XPS) to characterise the polymer formed.[17] Here, Raman spectroscopy was used to confirmed by the presence of bands assigned to C–C skeletal stretching (629 cm^{-1}), delta C–C–C stretching (348 cm^{-1}), NH_2 wagging (1228 cm^{-1})/bending (1568 cm^{-1}) and CH_2 bending (1480 cm^{-1}), which is consistent with spectra of PAm reported in literature (Fig. 2C).[29] Furthermore, SEM-EDX analysis of PAm features (Fig. S13, ESI†) confirmed the deposition of organic material with strong signals for C (carbon), N (nitrogen), and O (oxygen) all present.

To explore the limits of the system, the reducing potential was changed from V_{surf} = −0.2 V to V_{surf} = −0.5 V (*vs.* Ag/AgCl) in 100 mV increments. This led to interesting *i vs. t* traces which showed an initial increase in current at the beginning of the polymerisation, follow by a sharp decrease in current to near zero values (Fig. 3A). This sharp fall in current has been observed previously when single-barrel nanopipettes, in the related scanning ion conductance microscopy (SICM), have been employed to electrochemically interrogate crystallization processes. Therein, the build-up of material in the aperture of probes resulted in 'blocking' and loss of the connection between the QRCE in the nanopipette and the one in the bulk solution.[30,31]

Here the 'blocking' is attributed to the formation of insulating PAm gel formed in the droplet and the barrel of the nanopipette leading to a sharp fall in current and eventual loss of the connection between the QRCE in the nanopipette and the electrode surface in this case (Fig. 3 and Fig. S14A–D and S15, ESI†). Plots of the average blocking time as a function of the V_{surf} (Fig. S14E, ESI†), indicated strong correlation between V_{surf} and the blocking time. The formation of the PAm gel occurs *via* FRP initiated by radicals formed through direct reduction of HEBiB at the electrode surface. Furthermore, the amount of Cu^{II}/TPMA deactivator, required to maintain control of the eATRP mechanism, would significantly decrease with decreasing V_{surf}.[32] The formation of these gel-type features is further evidence that is it possible to prepare PAm using SECCM. More significantly, it indicates that there is also a distinct mechanistic shift from a regime of controlled eATRP to uncontrolled FRP which occurs at $V_{surf} \approx -0.2$ V. This represents significant progress compared to our previous work in which competing initiation mechanisms could not be decoupled.[17]

Finally, to highlight the potential of performing localised eATRP of Am using single-channel SECCM, a self-assembled monolayer (SAM) of bis[2-(2-bromoisobutyryloxy)ethyl] disulphide was formed on the gold substrate (Fig. S1, ESI†) to carry out surface-initiated eATRP (SI-eATRP). CV was performed on a droplet cell formed on the SAM-functionalised gold electrode. Pleasingly a reduction event with an onset of E = −0.06 V, assigned to reduction of Cu^{II}/TPMA to Cu^{I}/TPMA followed by activation of the surface bound initiator, was observed (Fig. S16, ESI†).

Localised SI-eATRP of Am was performed by bringing a nanopipette, containing an aqueous solution of Cu^{II}/TPMA

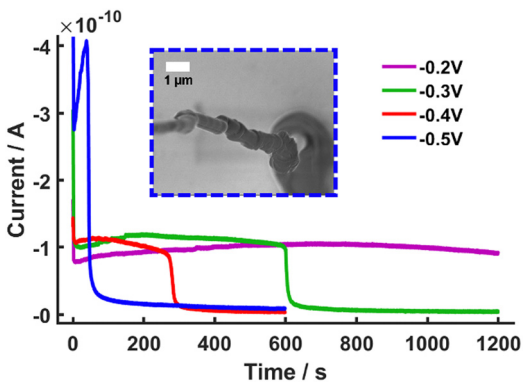

Fig. 3 *i vs. t* plots recorded during the potentiostatic (E_{app} = −0.20 − (−0.50) V) single-barrel SECCM eATRP/FRP of Am using [Am] : [HEBiB] : [Cu^{II}] : [TPMA] = [20] : [1] : [0.5] : [0.625]; (inset) SEM image of a gel-like feature formed when E_{app} = −0.50 V.

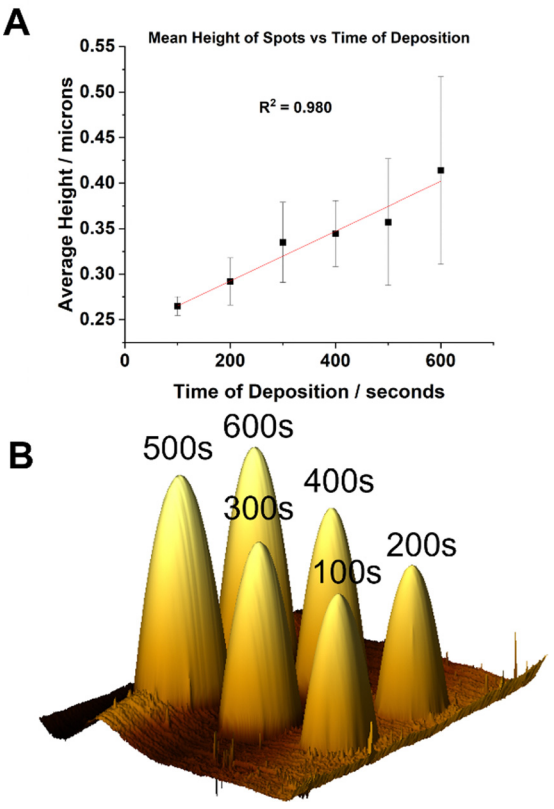

Fig. 4 Si-eATRP of Am at a SAM-functionalised gold electrode using [Am] = 10 wt% and [Cu^{II}/TPMA] = 6.9 mM; (A) feature height as function of reaction time; (B) 3D representation of the AFM image of features deposited at E_{app} = −0.15 V at increasing reaction times (100–600 s).

(6.9 mM) and Am (10 wt%), to the SAM-functionalised surface biased at $V_{surf} = -0.15$ V. The period of the time the meniscus was held at the SAM surface was increased from 100 s to 600 s in 100 s increments. A linear correlation between reaction time and the average feature height was observed which is indicative of good control over polymer brush growth (Fig. 4A and B; Fig. S17 and S18, ESI†).[33] There was very little change in the radial dimensions of the features formed (Fig. S19, ESI†). This provides additional evidence for PAm brush growth occurring perpendicular to the surface which has less of an effect on surface wettability compared to the synchronous synthesis and deposition of PAm at virgin gold electrode surfaces (*vide supra*). The features formed on the SAM-functionalised gold substrate remained after an aqueous rinse, providing strong evidence of SI-eATRP occurring from the initiator bound to the gold surface (Fig. S17, ESI†).

In conclusion, single-barrel SECCM has been employed to achieve localised eATRP of Am in droplet cells formed at gold electrode surfaces. The use of Cu^{II}/TPMA, provides control over the polymerisation whilst a mechanistic shift from eATRP to FRP has been observed at $V_{surf} \approx -0.2$ V, with eATRP favoured at $V_{surf} > -0.2$ V. SI-eATRP of Am from a SAM-functionalised gold electrode surface demonstrated control over the PAm brush height formed as a function of reaction time. This has highlighted the potential of single-barrel SECCM for the localised synthesis and deposition of soft materials. It also provides a simple and efficient platform to screen potential polymerisation conditions for translation to dual-barrel SECCM which can be used for more complex patterning of substrates.

The authors thank the Polymer Characterization and Microscopy Research Technology Platforms. P. W. thanks the Royal Society and Tata companies (URF\R1\180274) and the EPSRC for funding (studentship, M. M.; EP/R513374/1). E. L. acknowledges the Institute of Advanced Studies and the Eutopia Science and Innovation Fellowship for funding (European Union's Horizon 2020 research and innovation programme under the Marie Skłodowska-Curie grant agreement No 945380).

Conflicts of interest

There are no conflicts to declare.

Notes and references

1 A. B. Braunschweig, F. Huo and C. A. Mirkin, *Nat. Chem.*, 2009, **1**, 353–358.
2 J. K. Patra, *et al.*, *J. Nanobiotechnol.*, 2018, **16**, 71.
3 A. Q. Zhang and C. M. Lieber, *Chem. Rev.*, 2016, **116**, 215–257.
4 Y. S. Zholdassov, D. J. Valles, S. Uddin, J. Korpanty, N. C. Gianneschi and A. B. Braunschweig, *Adv. Mater.*, 2021, **33**, e210080.
5 B. D. Gates, Q. Xu, M. Stewart, D. Ryan, C. G. Willson and G. M. Whitesides, *Chem. Rev.*, 2005, **105**, 1171–1196.
6 B. Li, M. He, L. Ramirez, J. George and J. Wang, *ACS Appl. Mater. Interfaces*, 2016, **8**, 4158–4164.
7 L. Shen, C. He, J. Qiu, S.-M. Lee, A. Kalita, S. B. Cronin, M. P. Stoykovich and J. Yoon, *ACS Appl. Mater. Interfaces*, 2015, **7**, 26043–26049.
8 M. Guardingo, P. Gonzalez-Monje, F. Novio, E. Bellido, F. Busque, G. Molnar, A. Bousseksou and D. Ruiz-Molina, *ACS Nano*, 2016, **10**, 3206–3213.
9 F. Huo, Z. Zheng, G. Zheng, L. R. Giam, H. Zhang and C. A. Mirkin, *Science*, 2008, **321**, 1658–1660.
10 N. Ebejer, M. Schnippering, A. W. Colburn, M. A. Edwards and P. R. Unwin, *Anal. Chem.*, 2010, **82**, 9141–9145.
11 C. L. Bentley, M. Kang and P. R. Unwin, *J. Am. Chem. Soc.*, 2017, **139**, 16813–16821.
12 C. L. Bentley, M. Kang, F. M. Maddar, F. Li, M. Walker, J. Zhang and P. R. Unwin, *Chem. Sci.*, 2017, **8**, 6583–6593.
13 P. M. Kirkman, A. G. Guell, A. S. Cuharuc and P. R. Unwin, *J. Am. Chem. Soc.*, 2013, **136**, 36–39.
14 K. McKelvey, M. A. O'Connell and P. R. Unwin, *Chem. Commun.*, 2013, **49**, 2986–2988.
15 H. V. Patten, L. A. Hutton, J. R. Webb, M. E. Newton, P. R. Unwin and J. V. Macpherson, *Chem. Commun.*, 2015, **51**, 164–167.
16 A. N. Patel, K. McKelvey and P. R. Unwin, *J. Am. Chem. Soc.*, 2012, **134**, 20246–20249.
17 E. E. Oseland, Z. J. Ayres, A. Basile, D. M. Haddleton, P. Wilson and P. R. Unwin, *Chem. Commun.*, 2016, **52**, 9929–9932.
18 B. Zhao, M. Mohammed, B. A. Jones and P. Wilson, *Chem. Commun.*, 2021, **57**, 3897–3900.
19 B. Zhao, F. Pashley-Johnson, B. A. Jones and P. Wilson, *Chem. Sci.*, 2022, **13**, 5741–5749.
20 B. Zhao, J. Cheng, J. Gao, D. M. Haddleton and P. Wilson, *Macromol. Chem. Phys.*, 2023, **7**, 2300039.
21 M. Mohammed, B. A. Jones and P. Wilson, *Polym. Chem.*, 2022, **13**, 3460–3470.
22 E. Daviddi, Z. Chen, B. Beam Massani, J. Lee, C. L. Bentley, P. R. Unwin and E. L. Ratcliff, *ACS Nano*, 2019, **13**, 13271–13284.
23 J. Hengsteler, B. Mandal, C. Nisselroy, G. P. S. Lau, T. Schlotter, T. Zambelli and D. Momotenko, *Nano Lett.*, 2021, **21**, 9093–9101.
24 V. Shkirskiy, L. C. Yule, E. Daviddi, C. L. Bentley, J. Aarons, G. West and P. R. Unwin, *J. Electrochem. Soc.*, 2020, **167**, 041507.
25 M. Fantin, A. A. Isse, K. Matyjaszewski and A. Gennaro, *Macromolecules*, 2017, **50**, 2696–2705.
26 N. Bortolamei, A. A. Isse, A. J. D. Magenau, A. Gennaro and K. Matyjaszewski, *Angew. Chem., Int. Ed.*, 2011, **123**, 11593–11596.
27 S. Park, P. Chmielarz, A. Gennaro and K. Matyjaszewski, *Angew. Chem., Int. Ed.*, 2015, **54**, 2388–2392.
28 M. Fantin, A. A. Isse, K. Matyjaszewski and A. Gennaro, *Macromolecules*, 2017, **50**, 2696–2705.
29 M. K. Gupta and R. Bansil, *J. Polym. Sci. Polym. Phys.*, 1981, **19**, 353–360.
30 F. M. Maddar, D. Perry and P. R. Unwin, *Crystal Growth Design*, 2017, **17**, 6565–6571.
31 D. Perry, A. S. Parker, A. Page and P. R. Unwin, *ChemElectroChem*, 2016, **3**, 2212–2220.
32 A. J. D. Magenau, N. Bortolamei, E. Frick, S. Park, A. Gennaro and K. Matyjaszewski, *Macromolecules*, 2013, **46**, 4346–4353.
33 B. Li, B. Yu, W. T. S. Huck, W. Liu and F. Zhou, *J. Am. Chem. Soc.*, 2013, **135**, 1708–1710.